Univerzita Komenského v Bratislave
Fakulta matematiky, fyziky a informatiky

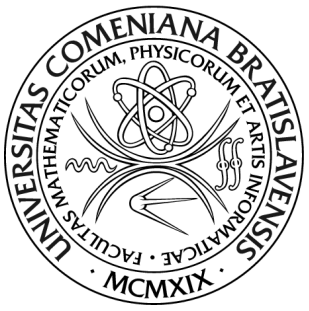

Pavol Mošať

Autoreferát dizertačnej práce

Study of spontaneous fission and K isomerism in rutherfordium isotopes

na získanie akademického titulu philosophiae doctor

v odbore doktorandského štúdia:

Jadrová a subjadrová fyzika

Bratislava, 2019

Dizertačná práca bola vypracovaná
v dennej forme doktorandského štúdia

na Katedre jadrovej fyziky a biofyziky

Predkladateľ:
Mgr. Pavol Mošať
Katedra jadrovej fyziky a biofyziky
Fakulta matematiky, fyziky a informatiky
Univerzita Komenského v Bratislave
Mlynská dolina
842 48 Bratislava

Školiteľ:
doc. Mgr. Stanislav Antalic, PhD.
Katedra jadrovej fyziky a biofyziky
Fakulta matematiky, fyziky a informatiky
Univerzita Komenského v Bratislave
Mlynská dolina
842 48 Bratislava

Študijný odbor: jadrová a subjadrová fyzika
Študijný program: 4.1.5. jadrová a subjadrová fyzika

Predseda odborovej komisie:
prof. RNDr. Jozef Masarik, DrSc.
Katedra jadrovej fyziky a biofyziky
Fakulta matematiky, fyziky a informatiky
Univerzita Komenského v Bratislave
Mlynská dolina
842 48 Bratislava

1 Introduction

The spontaneous-fission process is believed to finally terminate nuclear stability at increasing proton numbers Z or extreme ratios Z/N in heaviest nuclei. In the region of the heaviest elements, the macroscopic part of fission barrier vanishes at $Z \gtrsim 104$ and the nuclear stability against spontaneous fission (SF) is provided only by microscopic effects of few MeV resulting from the nuclear shell structure [1]. Investigation of structure and decay properties of the heaviest nuclei is essential in order to determine the production possibilities of superheavy isotopes, to understand the limits of nuclear stability and to improve models predicting next spherical proton and neutron shells beyond ^{208}Pb ($Z = 82, N = 126$). The study of spontaneous-fission properties such as fission-fragment mass distributions, total kinetic energies, prompt neutron emission and partial half-lives of the isotopes from the transfermium region presents a challenge for nuclear physics nowadays [2].

In this region only some basic experimental information on half-lives or branching ratios is available. The knowledge about fission modes, kinetic energy release and mass distribution of fission fragments is scarce. Especially interesting are total kinetic energy (TKE) measurements, that are connected to the fission mode (asymmetric from elongated shape, symmetric from elongated or compact shape). The experimental values of mean TKE and also TKE distributions are very valuable inputs for theoretical descriptions of SF.

Measurements of TKE distributions revealed the possibility of bimodal fission, with two fission modes, for several isotopes in trans-uranium region. Theoretical calculations discuss the possibility of bimodal fission for even $^{254\text{-}260}$Rf isotopes, which should be noticeable in their TKE distributions [3]. Experimental studies of mass and TKE distributions confirmed the concept of bimodal fission in lighter nuclei up to nobelium (e.g. ^{258}Fm, ^{259,260}Md or ^{258,260}No) [4, 5]. Only few results with limited statistics of SF events with total kinetic energy were obtained for rutherfordium ($Z = 104$) isotopes until now [4, 5, 6].

In this work we present data on SF of ^{255}Rf, ^{256}Rf, and ^{258}Rf obtained at SHIP, where fragment energies from the SF of nuclei implanted in a silicon detector were measured. To evaluate the mean TKE, it was necessary to correct the detector response for the energy deficit, mainly due to the pulse height defect.

Another interesting feature studied in this region is the presence of isomeric states. Detailed spectroscopic studies of nuclei near the deformed shells $Z = 100$ and $N = 152$ where the presence of K isomers was found, serve us as a strong tool for investigations into the structure of the heaviest elements.

The existence of K-isomeric states was previously confirmed in several even-even isotopes (e.g. ^{252}No [7], ^{254}No [8, 9, 10], ^{254}Rf [11], ^{256}Rf [12, 13]), and odd-even or even-odd isotopes (e.g. ^{253}No [14, 15], ^{255}Lr [16, 17], ^{257}Rf [18]).

In ^{255}Rf, a single-particle $5/2^+[622]$ isomer with $T_{1/2} = 50 \pm 15\,\mu$s populated by α decay of ^{259}Sg was previously identified with an excitation energy of $\approx 135\,$keV [6]. However, the presence of K isomer in ^{255}Rf was not confirmed up to now.

1.1 Goals of thesis

The main goal of this work was to investigate the SF properties of isotopes ^{255}Rf, ^{256}Rf, and ^{258}Rf produced at fusion-evaporation reactions ^{50}Ti + ^{207}Pb, ^{50}Ti + ^{208}Pb and ^{50}Ti + ^{209}Bi. Part of the measurements was carried out in 2014 at GSI using the accelerator UNILAC and the velocity filter SHIP. The aim of these experiments is to obtain new data on the nuclear structure and on the production mechanism. Up to now there is a lack of satisfying data on SF properties of Rf isotopes. We focused our interests on the evaluation of $\overline{TKE}$ and energy distribution in respect to expected bi-modal fission. The other goal was to investigate the isotope of ^{255}Rf for the presence of K isomers, which were confirmed in its neighbouring isotopes. For this purposes the same data were used.

2 Physical background

2.1 Total kinetic energy release in spontaneous fission

The electrostatic interaction between two fission fragments of positive charges given by proton numbers Z_1 and Z_2 can be described as

$$TKE = Z_1 Z_2 e^2 F(r) \tag{1}$$

where $F(r)$ depends on the fragments shape and charge distribution during scission.

The mutual repulsion can be written as

$$TKE = \frac{\left(\frac{Ze}{2}\right)^2}{2R} = \frac{e^2}{2^{8/3} r_0}\left(\frac{Z^2}{A^{1/3}}\right) \tag{2}$$

where the nuclear radius was expressed as $R = r_0(A/2)^{1/3}$ with r_0 nuclear radius parameter [19]. The dependence of the $\overline{TKE}$ experimental data on the $\frac{Z^2}{A^{1/3}}$, a.k.a. Viola-Seaborg systematics, is shown in Fig. 1. The $\overline{TKE}$ of asymmetrically fissioning isotopes is linearly increasing with $\frac{Z^2}{A^{1/3}}$. The group of symmetrically fissioning isotopes shows increased values of $\overline{TKE}$ and does not fit to the linear trend.

From fitting of the experimental data to Eq. 2 the value of 1.8 fm for nuclear radius parameter can be extracted instead of typical $r_0 = 1.2 - 1.3$ fm. The most convincing explanation is based on the strong prolate deformation of fission fragments after the scission [19].

2.2 Bimodal fission

Measurements of TKE distributions revealed the possibility of bimodal fission for several isotopes in trans-fermium region. The phenomenon of bimodal fission can be explained as a coexistence of two fission modes for the SF of an isotope. These two modes are characterized by significantly different $\overline{TKE}$. The calculations of potential-energy surfaces revealed two different paths to fission, the first following

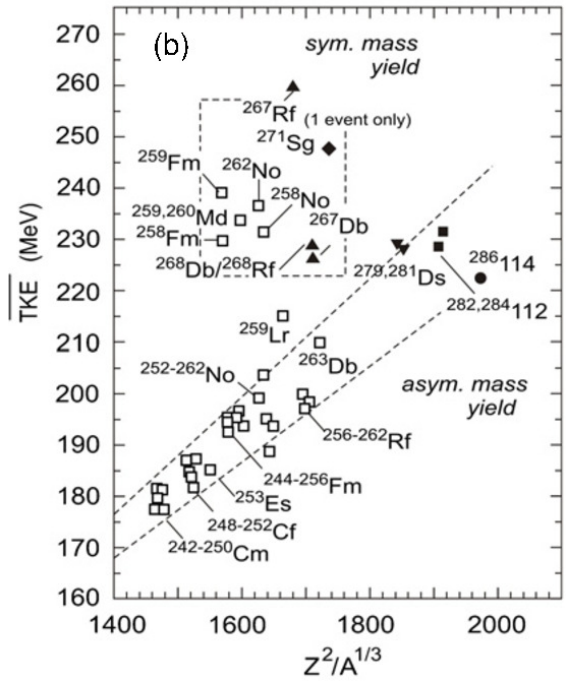

Figure 1: $\overline{TKE}$ from spontaneous fission variation with $\frac{Z^2}{A^{1/3}}$ [20].

the liquid-drop model and the second influenced by shell effects. The liquid-drop model like path leads to a fission from elongated shapes of fission fragments at the scission point. This fission mode is typically characterized by lower $\overline{TKE}$ values. The shell-effect path leads to a fission from compact shapes and the $\overline{TKE}$ are higher by ≈35 MeV. The competition of these two modes and thus a visible change in measured $\overline{TKE}$ is discussed in recent theoretical calculations where the possibility of bimodal fission for even Fm and Rf isotopes is reported [3].

Experimental studies of mass and TKE distributions confirmed the concept of bimodal fission in lighter nuclei up to nobelium (e.g. ^{258}Fm, ^{259,260}Md or ^{258,260}No) [4, 5]. However until now, only few results with limited statistics of SF events with measured total kinetic energy were obtained for rutherfordium ($Z = 104$) isotopes [4, 5, 6].

2.3 Nuclear isomerism

Nuclear isomers are long-lived metastable states of atomic nuclei. Nuclear isomers consist of the same nucleons, but with different orbital configuration. Typical excitation energies may reach up to several MeV. The existence of the isomers itself is allowed when there is a secondary minimum in the potential energy dependence on some nuclear variables, such as shape elongation, spin or the projection of spin into the symmetry axis (see Fig. 2). When a nuclei find itself in the secondary minimum, a small change in one of nuclear variables may lead only to state with higher excitation energy. A transition which would lead to energetically more favourable state demands a large change in either shape elongation or spin or spin projection.

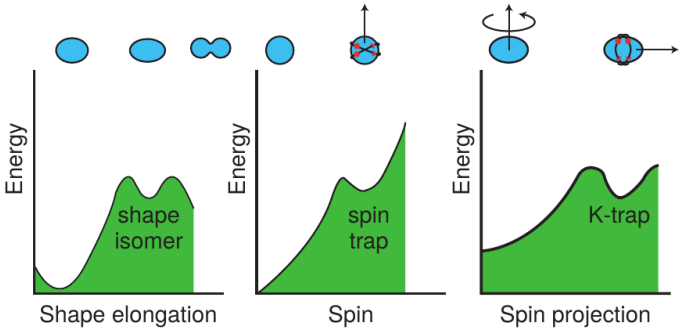

Figure 2: Three types of isomers [21].

2.3.1 K isomers

In deformed, axially symmetric nuclei, the quantum number K is defined as the projection of total nuclear spin Ω, onto the symmetry axis. By breaking nucleon pairs, multi-quasiparticle (qp) configurations with high-K value are possible. The selection rules for electromagnetic transitions require the multipolarity of the decay radiation at least as large as the change in the K value [22]. These rules give rise to K isomers, the metastable, relatively long-lived states with high K. Detailed spectroscopic studies of nuclei near the deformed shells $Z = 100$ and $N = 152$, where the presence of K isomers was found, serve us as a strong tool for investigations into the superheavy elements properties. High-K isomers are of special interest with respect to the properties of superheavy isotopes as their hindrance against spontaneous fission or alpha decay may lead to existence of states exceeding the lifetime of the ground state. An example can be found in ^{270}Ds with reported half-lives for the ground state and high-K isomeric states $100^{+140}_{-40}\mu$s and $6.0^{+8.2}_{-2.2}$ms, respectively [23].

In the transfermium region, the existence of K-isomeric states was previously confirmed in several even-even isotopes (e.g. ^{252}No [7], ^{254}No [8, 9, 10], ^{254}Rf [11], ^{256}Rf [12, 13]), and odd-even or even-odd isotopes (e.g. ^{253}No [14, 15], ^{255}Lr [16, 17], ^{257}Rf [18]).

2.4 Compound nucleus reactions

The idea of compound nucleus reactions (a.k.a. reactions of complete fusion or fusion-evaporation reactions) is based on an assumption that a projectile a accelerated to the energy T_α (in laboratory system) hits the stationary target nucleus X in a way that the impact parameter is small compared to the size of nucleus. Projectile overcomes the Coulomb barrier and enters the target nucleus. The projectile kinetic energy is redistributed among all nucleons and a heavier system called compound nucleus (CN) is formed. The probability of the formation process depends on the energy of incident projectile and available quantum levels in the target nucleus. After the energy redistribution, the CN is in a state of high excitation and high angular momentum. The de-excitation is done firstly by the emission of protons, neutrons

and alpha particles and later by γ quanta. The rest of the CN after the evaporation and final de-excitation is called "evaporation residue" (ER) and can be considered as the final product of the reaction. The CN formation takes $\sim 10^{-22}$ s. The whole process can be schematically represented as

$$a + X \longrightarrow CN^* \longrightarrow Y + b \tag{3}$$

where the b can be understood as all evaporated particles (protons, neutrons, α) from the CN. The a (projectile) and X (target) represent input channel of the reaction, while the Y and b are output channel. In CN^* the asterisk stands for the excited state. The excitation energy can be approximately defined as

$$E^* = Q + (\frac{m_X}{m_X + m_a})T_a \tag{4}$$

where the Q value of the reaction is

$$Q = (m_a + m_X - m_{CN^*})c^2 \tag{5}$$

and m_a, m_X and m_{CN^*} are the masses of projectile, target and compound nucleus. Typically $E^* = (30 - 60)$ MeV. The average binding energy per nucleon for heavy nuclei is about $(7 - 8)$ MeV. Although the incident projectile bring significant amount of energy to the CN, it is redistributed among $200 - 250$ nucleons. The average gain of energy per nucleon is insufficient for any nucleon to escape the nucleus. Due to the random collisions between nucleons it is possible that enough amount of energy will be concentrated into one nucleon which can be evaporated. The process of nucleon emission takes $\sim 10^{-19}$ s. Later ($\sim 10^{-17} - 10^{-10}$ s) the evaporation residue is de-exciting by the emission of γ quanta until it reaches the ground state.

3 Experimental setup

3.1 Velocity filter SHIP

SHIP (Separator for Heavy Ion reaction Products) uses specific kinematic properties of fusion-evaporation reaction products to separate them from projectiles that did not react in the target and from other undesired produced nuclei. The separator (configuration showed in Fig. 3) is placed in the direction of beam from UNILAC (UNIversal Linear ACcelerator).

The accelerator is able to produce stable heavy ion beams from carbon to uranium of intensities up to 10^{13} particles / s with energies up to 20 MeV / u. It is working in pulsed mode of 50 Hz. One 20 ms macropulse consists of 5 ms long beam burst and 15 ms period without beam called "pause".

Projectiles are directed to the target material mounted on a rotating wheel construction. Due to the diffraction the reaction products leave the target under a wide range of angles from the direction of primary beam. A triplet of quadrupole magnets is used to focus these deflected evaporation residues. Each of the quadrupole magnets is turned by 120° to obtain a uniform focusation.

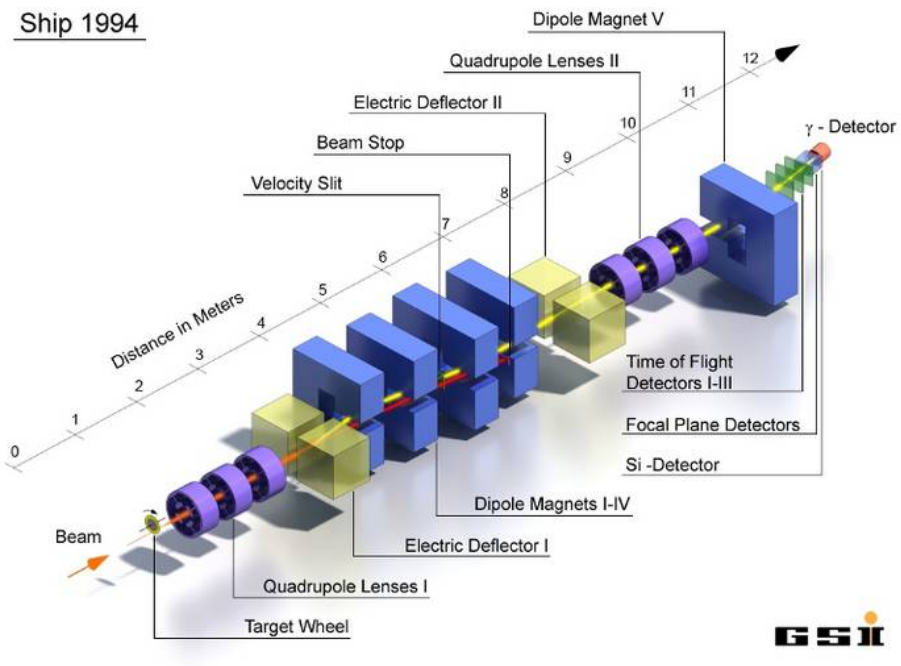

Figure 3: Velocity filter SHIP [24].

The reaction products are escaping the target with the velocities lower than the velocities of projectiles of primary beam that are simply passing through the target without interacting. After the interaction, compound nuclei have the same momentum as incident projectiles since the target nuclei are not moving in the direction of beam and thus their contribution to the momentum of compound nuclei is zero.

Different velocities are the main principle used in the separator. The velocity filter itself consists of electrical deflecting plates and magnetic dipoles. In opposite to the usual Wien filters, SHIP works with separated fields organized as electrostatic deflector I + 2 magnetic dipoles I and II followed by a mirror reversed configuration, 2 magnetic dipoles III and IV + electrostatic deflector II. Another triplet of magnetic quadrupoles is placed after the separator in order to focus the particles that did pass through the separator. The beam of separated particles is then deflected with a magnetic dipole V by 7.5° for the background suppression reasons [25].

3.2 Detectors

Selection of suitable detectors depends on the type of detecting particles, their energies, type of expected radioactive decay, half-life, intensity, etc. Neutron deficient isotopes in the transfermium region produced at SHIP are mostly undergoing α decay, SF and EC/β^+ decay with a wide range of half-lives (from microseconds to minutes). Spontaneous fission is always accompanied by the emission of γ rays and so is the de-excitation of possibly present isomeric states (even though the de-excitation by internal conversion is in many cases more probable and accompanied

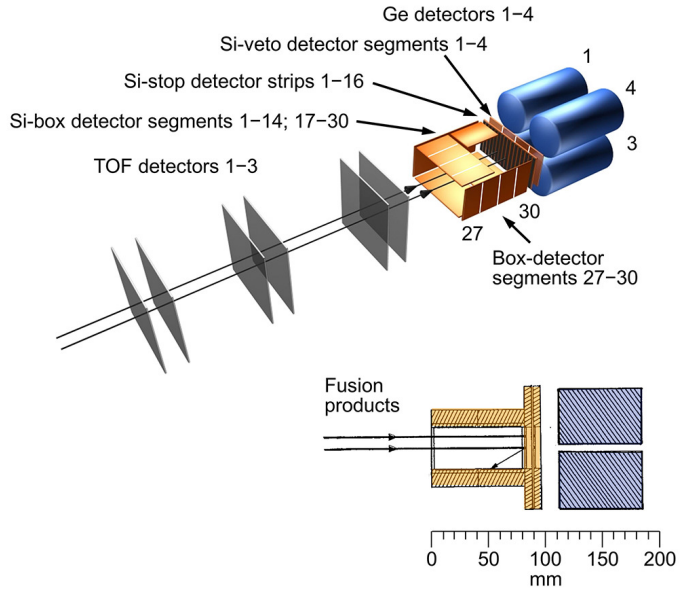

Figure 4: Detection system at velocity filter SHIP [26].

by X-rays and Auger electrons). The detection system at SHIP in Fig. 4 was built to fulfill these demands as much as possible.

TOF

The evaporation residues firstly pass through a triplet of TOF detectors [27]. Each of three TOF systems consists of a carbon foil of $55\,\mathrm{cm}^2$ surface and $30\,\mu\mathrm{g/cm}^2$ thickness and a parallel mesh. Electric potential difference between the foil and the mesh creates an accelerating electric field $\vec{E}$. A perpendicular homogeneous magnetic field $\vec{B}$ is also applied. Evaporation residues passing through the carbon foil eject electrons which are accelerated by $\vec{E}$. The presence of $\vec{B}$ is twisting the electron direction into the circular motion. The electrons are directed into the micro-channel plates where they are collected creating a signal. One of the main purposes of this detectors is to distinguish between implanted particles (with TOF signals) and particles from the decay (without TOF signals) and thus suppress the background in spectra. The types of particles (e.q. evaporation residues, transfer products, projectiles,...) flying through the TOF system can be distinguish using their different kinematic properties - different time-of-flights and energies.

STOP

Evaporation residues that passed through the separator and TOF system are implanted into the position-sensitive silicon strip detector with 16 strips also called as the "STOP" detector. Each of the strips represents an individual y-position sensitive detector 5 mm wide and 35 mm long. The active area of the whole STOP detector is $80 \times 35\,\mathrm{mm}$. Considering the y position resolution of each strip (about

150 μm FWHM for an α source) the system behaves as a set of 3700 small detectors with dimensions 5×0.15 mm. For an external α source of ^{241}Am the energy resolution is about 14 keV. In real situations when α particles are emitted by an implanted evaporation residue in the STOP detector, the FWHM is worsen a little bit to $(20 - 25)$ keV.

BOX

The system of six silicon strip detectors organized in "box" geometry is placed just in front of the STOP detector in order to detect particles escaping from the STOP detector in backwards direction. This configuration provides geometrical efficiency of 80 % from 2π half-space in front of the STOP detector.

CLOVER

The detection of γ rays and X-rays is achieved by the CLOVER detector composed of four Ge crystals, which is installed very close behind the STOP detector.

3.3 Some remarks on detection of SF activities using SHIP detection setup

The implantation depth of ERs into the focal plane detector is typically a few µm while the range of fission fragments in silicon is 10–20 µm. When registering SF of evaporation residues implanted in the STOP detector, three different situations can occur. Considering a 180° angle between the fission fragments, there is ≈ 60% probability (strongly depending on the ER implantation depth in the STOP detector) that both fragments are stopped in the STOP detector [Fig. 5a)]. The remaining part are events (≈ 40% of all) when one fragment escapes from the STOP detector in backward direction. In this case there is ≈ 80% probability for the escaped fragment to be detected by the BOX detector [denoted here as STOP-BOX coincidences; see Fig. 5b)]. The remaining ≈ 20% of the escaping fragments are not fully detected [Fig. 5c)]. Since fission events with one escaped fragment not registered by the BOX cannot be separated from the events with both fragments being stopped in the STOP detector, we refer to both cases as "STOP-BOX anticoincidences". In the cases with one fragment completely escaped from the detection system, the fission energy cannot be fully reconstructed. The presence of these events in the spectrum results in a low-energy tail (for more details see [28]).

3.4 Time and position correlations

The produced nuclei are implanted into the focal plane detector at SHIP experiment. The identification of an isotope is usually done within our experiment by the use of time and position correlation method [29]. The method is based on a search of subsequent decays originating from the place of ER implantation. The signals from the ER implantations are measured in the high-energy branch of electronic system.

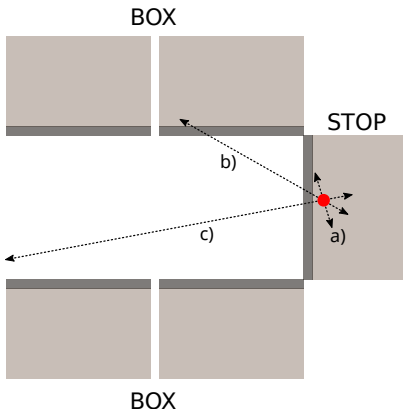

Figure 5: Schematic view (not to scale) of STOP and BOX detectors registering fragments from SF of an implanted nucleus (side view with respect to the direction of implantation). Red circle represents an evaporation residue implanted into the STOP detector, arrows represent the directions of 2 fission fragments. Active area of Si detectors is in bright grey color, dead layers are in dark grey. From the geometrical point of view, three possible cases can occur:
a) STOP-BOX anticoincidence (both fragments stay in STOP),
b) STOP-BOX coincidence (one fragment escapes to BOX),
c) STOP-BOX anticoincidence (one completely escaped fragment).

At the same position subsequent decay/s of ER (and then decays of daughter nuclei) is/are expected according to the ER (and daughter nuclei) half-life and branching ratios. A chains of signals consisting of ER implantation and/or multiple subsequent decays are possible.

4 Experiment

Experiments aimed at the production of rutherfordium and dubnium ($Z = 105$) isotopes and investigations of their decay properties were carried out at GSI Darmstadt (Germany) using the velocity filter SHIP [30]. The beam of ^{50}Ti ions was accelerated by the UNILAC to energies from 225 to 243 MeV. The isotopes ^{255,256,258}Rf were produced in the fusion-evaporation reactions $^{50}\mathrm{Ti} + {}^{207,\,208}\mathrm{Pb}$ and $^{50}\mathrm{Ti} + {}^{209}\mathrm{Bi}$. Targets of ^{207}PbS, ^{208}PbS and $^{209}\mathrm{Bi_2O_3}$ with thicknesses of 450 µg/cm^2, 450 µg/cm^2 and 463 µg/cm^2, respectively, were used. The evaporation residues ^{255}Rf and ^{256}Rf were produced in the $2n$ evaporation channel from the compound nuclei while the ^{258}Rf was produced indirectly through the electron capture (EC) decay of ^{258}Db [31]. The details of irradiations are summarized in Table 1.

4.1 Correction of the energy deficit in TKE measurements

A crucial task for the evaluation of $\overline{TKE}$ using silicon detectors is the correction of the deficit in the measured energies. Two main effects influencing the TKE

Fusion-evaporation reaction	E_{beam} [MeV]	E_{targ} [MeV]	E^*_{CN} [MeV]	Time [Hours]	σ [nb]
^{207}Pb(^{50}Ti, 2n)^{255}Rf	243	239.8	23.4	33.4	11.4 (18)
^{208}Pb(^{50}Ti, 2n)^{256}Rf	233	229.8	15.8	17.2	2.4 (3)
	241.5	238.3	22.6	8.1	15.5 (17)
^{209}Bi(^{50}Ti, 1n)^{258}Db $\xrightarrow{EC}{}^{258}$Rf	236	232.6	16.0	195.6	2.9 (9)

Table 1: Summary of the individual irradiations during R292 at SHIP. From left to right, reaction is noted, E_{beam} is the beam energy before enetring the target, E_{targ} is the beam energy in the middle of target, $E*_{CN}$ is excitation energy of compound nucleus, then absolute time of measurements and calculated cross-sections are stated.

measurements were discussed in previous studies performed at SHIP [32, 33, 28].

First, the energy calibration of the silicon STOP and BOX detectors was based on α-decay energies of implanted nuclei. In contrast to signals from α particles, there is a pulse-height defect present for heavy ions (thus also fission fragments), see e.g. [34]. This effect is caused by non-ionizing interactions with atoms in the detector and recombination of electron-hole pairs and brings an energy deficit. Secondly, there is a strong dependence of the energy deficit on the implantation depth into the STOP detector. When fragments escape (for both STOP-BOX coincidences), they pass through the dead layers of STOP and BOX detector under various angles, which also contributes to the energy deficit.

In order to evaluate the energy deficit, we did a reanalysis of the data from [28], where the calibration reaction ^{48}Ca + ^{206}Pb was performed to produce ^{252}No for which a value of $\overline{TKE}$ = 194.3 MeV is known from previous studies [5]. We measured the $\overline{TKE}$ of ^{252}No at six different implantation depths for STOP-BOX anticoincident [Fig. 6a)] and coincident SF events [Fig. 6b)]. Experimental values of $\overline{TKE}$ were fitted by a saturation-growth function (see Fig. 6). The calculations of energy losses of ^{48}Ca projectiles in the target material (we considered reaction in the middle of the target thickness) as well as the losses of ^{252}No ERs in the target material, target backing foil, degrader foil and implantation depths in the STOP detector were done using LISE++ [35]. The energy deficit at given implantation depth can be determined as an energy difference of the known $\overline{TKE}$ of 194.3 MeV and the value from experimental fit as $\Delta E = (194.3 - \overline{TKE}_{fit})$ MeV.

4.2 Correction of the electron energies

For fast decays in our STOP detector (up to 500 µs) the signal from decay [e.g. α decay or internal conversion electrons (CE)] is summed with the tail of ER signal. This pile-up effect causes a deviation of measured decay energy and depends on the time difference between the decay and the ER implantation. For studies of electron energies in our work, discussed further in Sec. 5.4, it was necessary to

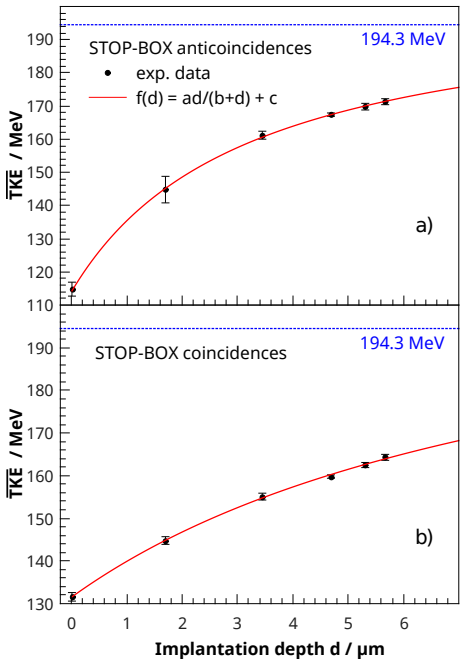

Figure 6: $\overline{TKE}$ from the SF of ^{252}No as a function of implantation depth of evaporation residues in the detector for: a) STOP-BOX anticoincident SF events, b) STOP-BOX coincident SF events. Blue dashed line: $\overline{TKE}$ = 194.3 MeV of ^{252}No from [5]. Red solid line: saturation-growth fit of experimental data.

determine an energy correction. We estimated this effect using the α decay of ^{216}Ac collected during the calibration measurement with reaction ^{50}Ti + ^{170}Er, which delivers a clearly separated peak at 9118 keV in the α spectrum and has a half-life of 440 ± 16 µs. The plot of measured α-particle energy as a function of the time difference between the implantation and decay is shown in Fig. 7. A clear dependence can be seen, influencing the energies of decays that occurred faster than 500 µs after the implantation of ER. After that time the energies saturate to the real value and the effect vanishes.

5 Results

We registered several hundreds of SF events in each of the irradiations. In order to identify the SF events of ^{255}Rf and ^{256}Rf isotopes, we used time and position-correlation methods [29] based on delayed coincidences between the ER implantation and subsequent high-energy signal (corresponding to SF) in the same position of the detector. For ^{258}Rf we also searched for conversion electrons after β decay of ^{258}Db produced in the reaction ^{50}Ti + ^{209}Bi and subsequent SF decay of the daughter nucleus ^{258}Rf. The searching time windows between either ER-SF or CE-SF were set to ≈ 5 time the half-life for each isotope. For the SF events, the energy condition for high-energy signals was set to 100–300 MeV. Searching methods and conditions as well as the statistics of detected SF events for each isotope are described in Sec. 5.1,

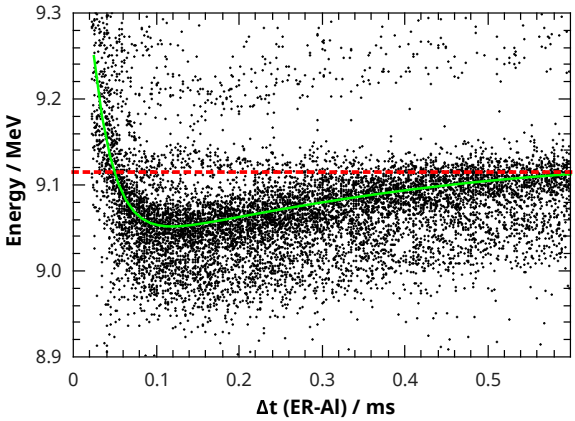

Figure 7: Measured energy of the ^{216}Ac α decay as function of the time after implantation of the ER. For fast decays, the signal from α decay is summed with the tail of ER signal. The correction is given as a difference between the fit of measured energies (green solid line) and expected energy (red dashed line) at given time.

Isotope	Event	Condition	$N_{(S-B)coinc}$	$N_{(S-B)anticoinc}$
^{255}Rf	ER-SF	$\Delta T = (35 - 8500)$ ms	160	715
^{256}Rf	ER-SF	$\Delta T = (0 - 35)$ ms	138	453
^{258}Rf	SF	γ coinc., BOX coinc.	220	-
^{258}Rf	CE-SF	$\Delta T = (0 - 60)$ ms	118	412

Table 2: Statistics of SF events for each isotope from STOP-BOX coincident (column IV) and anticoincident events (coulmn V). The searching time windows between either ER-SF or CE-SF are stated in column III. For the SF events, the energy condition for high-energy signals was set to 100–300 MeV.

5.2, and 5.3 and summarized in Table 2. We also searched for ER-CE-SF/α and ER-CE-CE-SF/α correlations in order to look for any possible isomers in ^{255}Rf. The details are described in Sec. 5.4.

5.1 ^{256}Rf produced in reaction ^{50}Ti + ^{208}Pb

The reaction ^{50}Ti + ^{208}Pb with the projectile energy set to 241.5 MeV (compound nucleus excitation energy of 22.6 MeV) was suited for the ^{256}Rf production through the $2n$ evaporation channel from the compound nucleus ^{258}Rf. For a part of the experiment the projectile energy was lowered to 232 MeV (compound nucleus excitation energy 15.0 MeV) to produce ^{257}Rf by $1n$ evaporation channel. In order to detect the SF events, we searched for ER-SF correlations. Together, we registered 591 SF events that were preceded by the implantation of ERs with time differences less than 35 ms corresponding to the half-life of ^{256}Rf ($T_{1/2} = 6.67$ ms [12]). In 138 cases they were in coincidence with BOX detector and the energy signal was reconstructed as a sum of signals from STOP and BOX detectors. We assigned all SF

events detected during this reaction to ^{256}Rf.

5.2 ^{255}Rf produced in reaction ^{50}Ti + ^{207}Pb

The next case was the study of ^{255}Rf produced in the reaction ^{50}Ti + ^{207}Pb via $2n$ evaporation channel from the compound nucleus ^{257}Rf. For this purpose, the beam energy was set to 243 MeV which corresponds to the compound nucleus excitation energy of 23.4 MeV. Similarly to reaction ^{50}Ti + ^{208}Pb, discussed in previous section, we also searched for ER-SF correlations. The minimum time difference between ER and SF signals was set to 35 ms in order to avoid a contamination from ^{256}Rf. The upper limit for the time window was set to 8500 ms, which is ≈ 5 times the half-life of ^{255}Rf (1.68 ± 0.09 reported in [36]).

In total, we identified 875 SF events corresponding to ^{255}Rf, 160 of them were in coincidence with BOX detector. Among these events we estimated the contribution of only 3 SF events that may originate from ^{256}Rf and as there is not any possibility for other SF activity, we assigned all SF events to ^{255}Rf.

5.3 ^{258}Rf produced via EC decay of ^{258}Db

The reaction ^{50}Ti + ^{209}Bi with the projectile energy set to 236 MeV ($E^*_{CN} = 16.0$ MeV) was suited for the ^{258}Db production through the $1n$ evaporation channel. A considerable amount of ^{258}Rf was produced by EC decay of ^{258}Db ($b_{EC} = 0.23 \pm 0.08$ and $T_{1/2} = 4.3 \pm 0.5$ s [10]). The investigations of the EC process in ^{258}Db and also α-decay studies of ^{258}Rf as well as the problematics of ^{258}Rf SF identification in this case were reported in [31, 37]. We searched for correlations between CE from the deexcitation of states in ^{258}Rf populated after the EC decay of ^{258}Db and subsequent SF.

We identified 530 SF events within a time window of 0–60 ms (≈ 5 times the half-life of ^{258}Rf [31]) between CE and SF. In 118 cases, signals were in coincidence with BOX detector. We assigned all events to ^{258}Rf. We estimated that the detection efficiency for electrons was less than 50%. Thus for further studies of STOP-BOX coincident events, we decided to take all high-energy events in coincidence with a signal from Clover detector (no correlation with CE) in order to increase the statistics in TKE distribution. The probability of STOP-BOX coincidence in the case of projectiles is very low, only due to the random coincidences and also projectiles are not accompanied by γ rays as it is in the case of SF events. Thus the criteria of STOP-BOX-CLOVER coincidence is strongly selective for SF detection [28]. We found 220 of these events, which almost doubled the statistics in comparison with CE-SF correlations. Since there is not any possible contribution from other SF activity we assigned all events to ^{258}Rf.

5.4 Search for isomeric states in ^{255}Rf

In order to look for new possible isomeric states in ^{255}Rf we searched for correlations containing an electron signal from the deexcitation of an isomeric state by internal

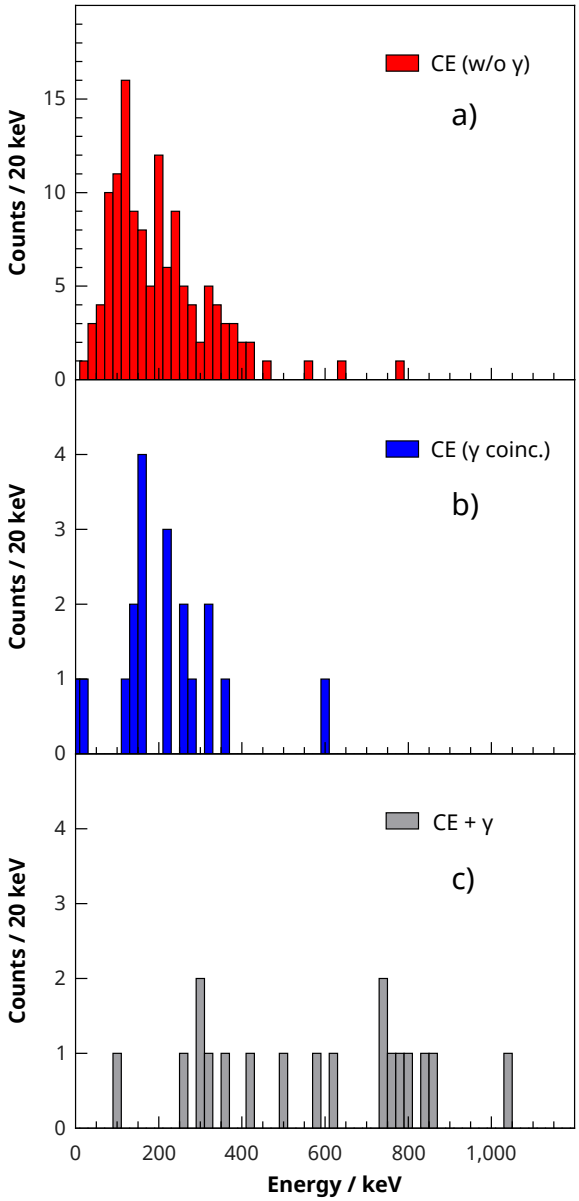

Figure 8: Energies of conversion electrons from the ER-CE-(CE)-SF/α correlations. a) electrons not coincident with γ rays, b) electrons in coincidence with γ rays, c) summed energies of electrons and coincident γ rays.

ER-CE-CE-SF/α chain	E_{CE1} [keV]	Δt_{CE1} [µs]	E_{CE2} [keV]	Δt_{CE2} [µs]	g.s. decay
1	81.0	57	147.5	33	SF
2	126.0	88	143.8	25	α
3	146.4	50	19.8	26	α

Table 3: Conversion electron characteristics from the ER-CE-CE-SF/α correlations.

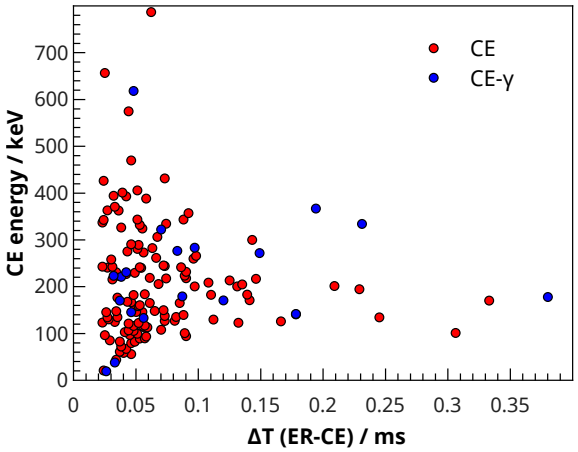

Figure 9: Conversion electron energies as a function of time difference between the implantation of ER and detection of CE. Red dots: electrons not in coincidence with γ rays, blue dots: electrons in coincidence with γ rays.

conversion, preceded by an ER signal and followed by an SF or α decay from the ground state (ER-CE-(CE)-SF/α). Conversion electrons were searched for in a time window of 500 µs after the ER implantation as a low-energy signal (up to 1 MeV). Subsequent α decays from the ground state (g.s.) of ^{255}Rf were searched for within 0–8500 ms and an energy range of 8500–9000 keV. For the SF, a time condition of 35–8500 ms was set in order to avoid the contamination of ^{256}Rf (with the same arguments that were mentioned in Sec.5.2).

We detected 144 ER-CE-SF/α correlations fulfilling the conditions mentioned above. In 74 cases chains ended by SF and in 70 cases by the α decay corresponding to ^{255}Rf or ^{251}No. The detection of ^{251}No α particles was preceded by 1–2 MeV signals originating from the escape of ^{255}Rf α particles from the detection system, ER-CE-α(^{255}Rf) or ER-CE-α(^{255}Rf)$_{esc.}$-α(^{251}No) correlations. We evaluated branching ratios of ^{255}Rf according to detector efficiencies to be $b_{SF} = 0.51 \pm 0.07, b_\alpha = 0.49 \pm 0.07$. A contribution of a branching ratio for EC decay of ^{255}Rf (evaluated as <0.06 in [6]) was not considered.

In three cases of detected ER-CE-SF/α correlations, the CE was followed by another CE within 500 µs. The details on these three ER-CE-CE-SF/α(^{255}Rf) correlations including CE energies and decay times for each chain are summarized in Table 3.

Isotope	$\overline{TKE}_{all}$ [MeV]	$\overline{TKE}_{ref}$ [MeV]	Ref.
^{255}Rf	199.5 ± 2.7	199 ± 3	[6]
^{256}Rf	198.7 ± 2.8	198.9 ± 4.4	[4]
^{258}Rf	198.2 ± 3.0	197.6 ± 1.1	[4]

Table 4: Total kinetic energies evaluated in this work, compared to previous results. In the table columns, from left to right, $\overline{TKE}$ of all events obtained from both STOP-BOX coincidences and anticoincidences, reference value of $\overline{TKE}$ and corresponding references are stated.

From the total of 147 CEs detected in ER-CE-SF/α or ER-CE-CE-SF/α correlations, in 19 cases, electrons were in prompt coincidence with γ rays and in 128 cases without. The energy spectra of these CEs without or with coincident γ rays are shown in Fig. 8a) and Fig. 8b) respectively. The CE energies were corrected by the method discussed in Sec. 4.2. Figure 9 shows the 2D plot of CE energies as a function of ER-CE time differences. We might separate the electrons into at least two groups according to their time distributions. The half-life of the lower-energy electrons (0–350 keV) is 35 ± 6 µs and the higher-energy group (> 350 keV) is 15 ± 5 µs.

6 Discussion

6.1 Total kinetic energies

As was mentioned in Sec. 3.3 the spectra from STOP-BOX anticoincidences contain a small part of events where one of the fragments escaped without being detected in the BOX detector. These events have incomplete energy and affect the shape of TKE distribution (see discussion in [28]). These distributions are therefore not suitable for the analysis of their shape as would be desirable for the search of bimodal fission, however they could still be scaled to allow us an evaluation of $\overline{TKE}$. The values of $\overline{TKE}$ obtained from all SF events (described in Fig. 5) for each isotope are summarized in Table. 4 and compared to results from previous studies. The $\overline{TKE}$ of ^{255}Rf isotope is 199.5 ± 2.7 MeV, which is in a good agreement with the value of 199 ± 3 MeV from [6], where ^{255}Rf was produced at SHIP indirectly by α decay of ^{259}Sg and the method from [33] was used to correct $\overline{TKE}$ for the energy deficit. The $\overline{TKE}$ values of 198.7 ± 2.8 MeV for ^{256}Rf and 198.2 ± 3.0 MeV for ^{258}Rf are also in a good agreement with previously measured 198.9 ± 4.4 MeV and 197.6 ± 1.1 MeV [4], respectively. The TKE distributions containing all types of SF events have $FWHM \approx 37$ MeV for all the three isotopes.

In order to study the shape of TKE distribution for bimodal fission search, it is necessary to use only STOP-BOX coincident events. These TKE distributions of ^{255}Rf, ^{256}Rf and ^{258}Rf are shown in Fig. 10. A slight asymmetry in the TKE

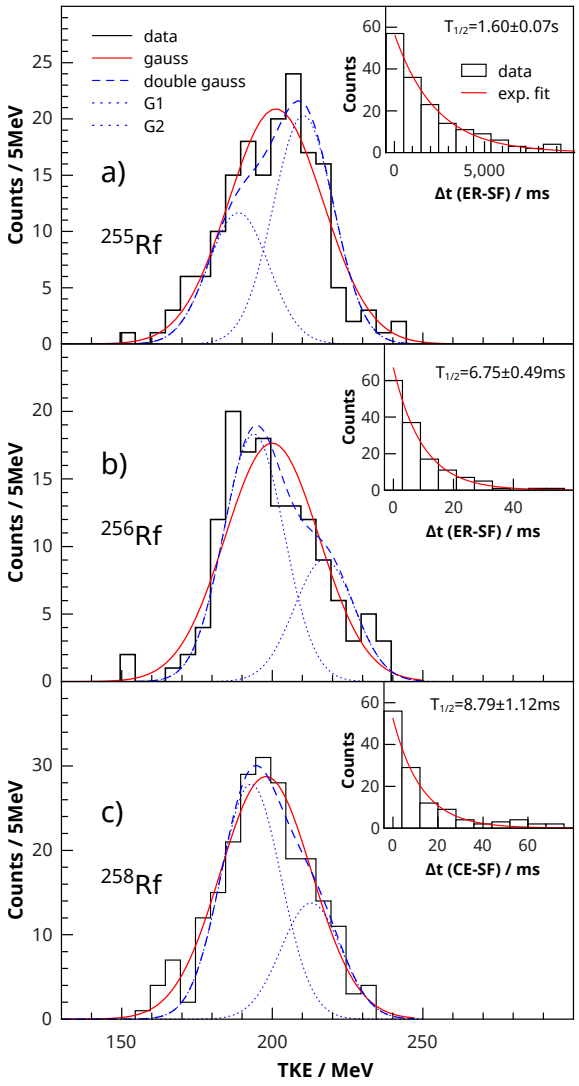

Figure 10: TKE distributions of SF fragments from STOP-BOX coincidences: a) for SF of ^{255}Rf obtained from ER-SF correlations (inset shows ER-SF time differences), b) for SF of ^{256}Rf obtained from ER-SF correlations (inset shows ER-SF time differences), c) for SF of ^{258}Rf obtained from STOP-BOX coincidences (inset shows CE-SF time differences in cases when CE was registered).

Isotope	Double gaussian fit				Single gaussian fit		
	$\overline{TKE}_L$ [MeV]	$\overline{TKE}_H$ [MeV]	ΔE [MeV]	χ^2/doF	$\overline{TKE}$ [MeV]	$FWHM$ [MeV]	χ^2/doF
^{255}Rf	186.3 ± 1.5	207.8 ± 0.8	21.8 ± 1.7	3.6	201.2 ± 0.9	31.3 ± 1.7	5.6
^{256}Rf	191.4 ± 0.7	214.8 ± 1.5	23.4 ± 1.9	3.3	197.5 ± 1.0	31.2 ± 2.0	6.7
^{258}Rf	194.4 ± 1.5	213.5 ± 4.8	19.1 ± 5.0	7.4	197.9 ± 0.7	30.3 ± 1.4	6.3

Table 5: In columns from left to right, for each isotope, characteristic values from fitting of TKE distributions (for SF events from STOP-BOX coincidences) are stated. For double-gaussian fit: $\overline{TKE}_L$ of low-energy component, $\overline{TKE}_H$ of high-energy component, ΔE energy difference between $\overline{TKE}_L$ and $\overline{TKE}_H$ and residual sum of squares (χ^2) divided by the degrees of freedom (doF). For single-gaussian fit: $\overline{TKE}$, FWHM and residual sum of squares (χ^2) divided by the degrees of freedom (doF).

distributions of ^{255}Rf and ^{256}Rf is noticeable. By fitting with single gaussian we obtained 201.2 ± 0.9 MeV with $FWHM = 31.3 \pm 1.7$ MeV and 197.5 ± 1.0 MeV with $FWHM = 31.2 \pm 2.0$ MeV for these two isotopes, respectively. By deconvolution with two gaussian components we estimated the $\overline{TKE}$ of low-energy and high-energy components to be 186.3 ± 1.5 MeV and 207.8 ± 0.8 MeV in the case of ^{255}Rf and 191.4 ± 0.7 MeV and 214.8 ± 1.5 MeV in the case of ^{256}Rf. The distribution for the isotope ^{258}Rf is more symmetric than the ones for ^{255}Rf and ^{256}Rf. The single-gaussian fit gives $\overline{TKE}$ of 197.9 ± 0.7 MeV with $FWHM = 30.3 \pm 1.4$ MeV, fit by two gaussians gives 194.4 ± 1.5 MeV and 213.5 ± 4.8 MeV.

The goodness of single- or double-gaussian fits can be characterised by the values of residual sum of squares (χ^2) divided by the degrees of freedom (doF). The χ^2/doF values of single- and double-gaussian fits for each isotope are stated in Table 5. Asymmetric TKE distributions and lower χ^2/doF values for double-gaussian fits lead us to the conclusion of possible bimodal fission for ^{255}Rf and ^{256}Rf. For ^{255}Rf the high-energy component is dominant while for ^{256}Rf the low-energy component is dominant. We note, however, that the positions of the two components are closer (energy differences ΔE are stated in Table 5) to each other in contrast to the bimodal fission in ^{258}Fm, ^{259,260}Md and ^{258,260}No [4, 5]. In ^{258}Rf we do not clearly see asymmetry in the TKE distribution and double-gaussian fit gives slightly higher χ^2/doF value than the single-gaussian fit.

6.2 *K* isomers in ^{255}Rf

A single-particle $5/2^+[622]$ isomer with $T_{1/2} = 50 \pm 15$ µs populated by α decay of ^{259}Sg was previously identified in ^{255}Rf with an excitation energy of ≈ 135 keV [6] based on the statistics of 42 ER(^{259}Sg)-α-CE correlations. None of the CEs in a previous study was observed in coincidence with γ rays. The energy distribution of the electrons formed a narrow peak at ≈ 105 keV with FWHM practically defined only by detector resolution. In our study, with direct production of ^{255}Rf, the

energy distribution of CEs from ER-CE-α/SF correlations was significantly broader and reaching up to 800 keV [see Fig. 8a)].

From all events in the energy range of 0–350 keV, 17 cases were detected in coincidence with γ rays, we evaluated their half-life as 38 ± 4 µs. Considering broader electron-energy distribution of these events in comparison with the study of $5/2^+[622]$ isomer in [6], the mean energy of ≈ 250 keV and many γ-coincident events, we conclude that we identified a new isomer, different from the reported single-particle $5/2^+[622]$ isomer.

In the energy range of 0–350 keV, we also found that most of the CEs were not in coincidence with γ rays. The half-life of these events was 35 ± 6 µs. The fact that many electrons were not in coincidence with γ rays can be explained by the γ-ray detection efficiency, however, there might be a contribution of CEs from the $5/2^+[622]$ isomer with $T_{1/2} = 50 \pm 15$ µs half-life for which no γ rays were observed in coincidence with CEs [6]. As these events result in similar half-lives and energies, they cannot be separated from the electrons originating in the deexcitation of the new isomer we identified. Thus for the estimations of the half-life and excitation energy of the new isomer we are discussing only electrons from the energy range 0–350 keV which were in coincidence with γ rays.

From the high number of electrons in comparison with the number of γ rays and non-observation of clear γ-ray peak, we assume that the transition deexciting the isomer has a high total conversion coefficient. However, for the low-multipolarity transitions high conversion coefficients are expected only for low transition energies up to 100–200 keV. Therefore, we consider our electron signals to be formed as a summed signal from a cascade of 3–5 transitions. The ground state of ^{255}Rf was assigned to be $9/2^-[734]$ state in [36] and thus the new isomer should be a high-K isomer with K number at least by 4–6 higher than the ground state. The excitation energy can be estimated from the summed energies of conversion electrons and coincident γ rays [Fig. 8c)], which go up to 1050 keV. Depending on the binding energies of electrons in the atomic K (≈ 147 keV) or L (≈ 29 keV) shells, the excitation energy is roughly estimated to 1150–1450 keV.

Another group of electrons with significantly different life-time was formed at energies above 350 keV (Fig. 9). The half-life of these events is $T_{1/2} = 15 \pm 5$ µs. Using the same arguments as above one can expect these signals to be the sum of an electron cascade from the deexcitation of another isomeric state with high K number. A supporting argument for an existence of two isomers is the observation of three ER(^{255}Rf)-CE-CE-SF/α correlations shown in Table 3. As the energies of electrons with $T_{1/2} = 15 \pm 5$ µs reach up to 800 keV one can estimate the excitation energy to be 900–1200 keV.

In all three cases of ER(^{255}Rf)-CE-CE-SF/α correlations from Table 3, the decay time of the first electron was longer than the decay time of the second one. Based on the results presented before we propose the tentative decay scheme shown in Fig. 11.

The crucial question for such an interpretation is the availability of levels to form a configuration with high K value. The scheme of available single-particle levels for protons and neutrons in ^{255}Rf prepared according to calculations from [38] with nuclear deformations taken from [39] is presented in Fig. 12. In this case

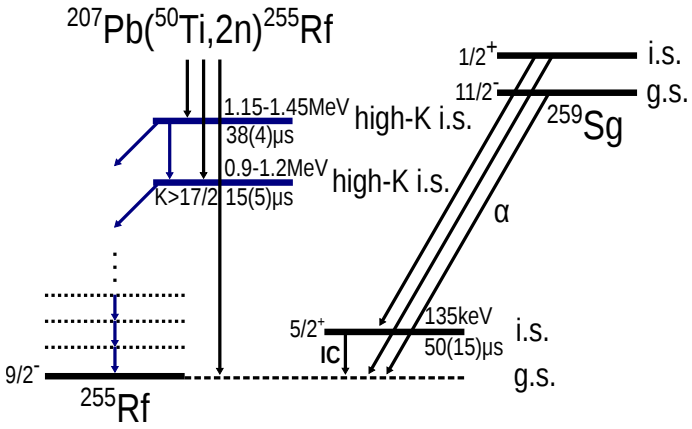

Figure 11: Proposed decay scheme of K-isomers in ^{255}Rf populated in the reaction ^{207}Pb(^{50}Ti,2n)^{255}Rf (left) and in the α decay of ^{259}Sg (right).

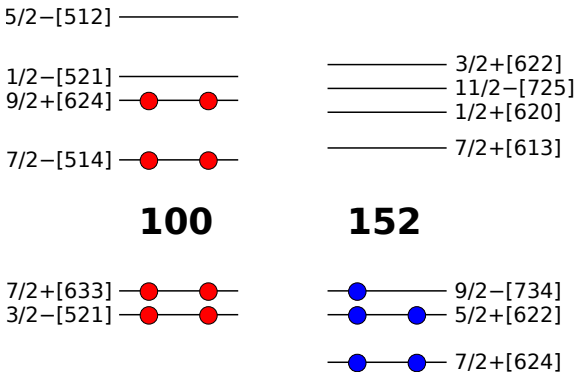

Figure 12: Single-particle levels for protons (left) and neutrons (right) in ^{255}Rf, calculated in [38] with nuclear deformations taken from [39]. Neutron level $5/2^+[622]$ was placed according to experimental results from [6]. The ground state configuration is shown.

a high-K configuration can be simply achieved for example by breaking a pair of protons at $9/2^+[624]$ or $7/2^-[514]$ and shifting one proton to the $1/2^-[521]$. Such three quasi-particle configurations $\{1/2^-[521]\pi \otimes 9/2^+[624]\pi \otimes 9/2^-[734]\nu\}$ and $\{1/2^-[521]\pi \otimes 7/2^-[514]\pi \otimes 9/2^-[734]\nu\}$ lead to $K = 19/2^+$ with $\Delta K = 5$ and $K = 17/2^-$ with $\Delta K = 4$. These and other examples of possible configurations with high-K are summarized in Table 6. The 3-qp configurations composed of three unpaired neutrons demand a neutron to be shifted over the level gap for deformed isotones at $N = 152$. From the estimations of excitation energy of new isomers, quite low-lying high-K state can be expected. Nevertheless, without having detailed calculations of energy gaps, one cannot exclude the possibility of three neutron qp state.

3-qp configuration	K^π	ΔK
$1/2^-[521]\pi \otimes 9/2^+[624]\pi \otimes 9/2^-[734]\nu$	$19/2^+$	5
$1/2^-[521]\pi \otimes 7/2^-[514]\pi \otimes 9/2^-[734]\nu$	$17/2^-$	4
$5/2^-[512]\pi \otimes 9/2^+[624]\pi \otimes 9/2^-[734]\nu$	$23/2^+$	7
$7/2^-[514]\pi \otimes 5/2^-[512]\pi \otimes 9/2^-[734]\nu$	$19/2^-$	5
$1/2^-[521]\pi \otimes 9/2^+[624]\pi \otimes 5/2^+[622]\nu$	$15/2^-$	4
$5/2^-[512]\pi \otimes 9/2^+[624]\pi \otimes 5/2^+[622]\nu$	$19/2^-$	5
$7/2^-[514]\pi \otimes 5/2^-[512]\pi \otimes 5/2^+[622]\nu$	$17/2^+$	4
$1/2^-[521]\pi \otimes 9/2^+[624]\pi \otimes 7/2^+[624]\nu$	$17/2^-$	4
$5/2^-[512]\pi \otimes 9/2^+[624]\pi \otimes 7/2^+[624]\nu$	$21/2^-$	6
$7/2^+[613]\nu \otimes 9/2^-[734]\nu \otimes 5/2^+[622]\nu$	$21/2^-$	6
$7/2^+[613]\nu \otimes 9/2^-[734]\nu \otimes 7/2^+[624]\nu$	$23/2^-$	7

Table 6: Examples of possible configurations of 3-qp high-K isomeric states in ^{255}Rf, according to single-particle levels calculated in [38] with nuclear deformations taken from [39] (see Fig. 12).

7 Conclusion

The thesis was focused on two topics. First, we studied the total kinetic energies of isotopes ^{255}Rf, ^{256}Rf, and ^{258}Rf and secondly, we investigated ^{255}Rf for the presence of K-isomeric states.

The energy calibrations of focal plane STOP detector as well as surrounding BOX detectors were done using the known α-particle energies from the decay of several isotopes produced in fusion-evaporation reaction ^{50}Ti + ^{170}Er. The main issue in measuring fission-fragment energies is the energy deficit caused by the pulse-height defect and detection geometry. In order to correctly evaluate the TKE of fission fragments from the spontaneous fission of Rf isotopes, we studied ^{252}No with known $\overline{TKE}$ implanted at different implantation depths in order to obtain response function of the detector system. For this purposes we reanalysed older data, where ^{252}No was produced in fusion-evaporation reaction with ^{48}Ca beam and ^{206}Pb target. We published this study in [40].

The correction of the energy deficit in TKE studied on the ^{252}No allowed us to evaluate the $\overline{TKE}$ of the rutherfordium isotopes ^{255}Rf, ^{256}Rf, and ^{258}Rf to be 199.5 ± 2.7 MeV, 198.7 ± 2.8 MeV and 198.2 ± 3.0 MeV, respectively. The results on $\overline{TKE}$ are in a good agreement with previous studies.

To investigate the TKE distributions for bimodal fission, we considered only STOP-BOX coincident events which guarantee the fully reconstructed energy of fission fragments. We observed asymmetric distributions for ^{255}Rf, ^{256}Rf and a more symmetric shape for ^{258}Rf. A possible explanation is the existence of bimodal fission for ^{255}Rf, ^{256}Rf, although weaker as in previous cases [4, 5]. Experimental results were also in a qualitative agreement with theoretical calculations [3].

During the study of ^{255}Rf, we were able to identify new high-K, presumably 3-qp, isomers with half-lives of $38 \pm 4\,\mu$s and $= 15 \pm 5\,\mu$s. We estimated the excitation

energies of these isomers to 1150–1450 keV and 900–1200 keV, respectively, with 150–300 keV of energy difference between them and a lower limit for spin of $17/2\hbar$. Based on these results we also proposed a tentative decay scheme. The details of this study were submitted for the publication [41].

References

[1] S. G. Nilsson, et al., *Nucl. Phys. A* **131**, 1 (1969).

[2] F. P. Heßberger, *Eur. Phys. J. A* **53**, 75 (2017).

[3] N. Carjan, et al., *Nucl. Phys. A* **942**, 97 (2015).

[4] J. F. Wild, et al., *J. Alloy. Compd.* **213**, 86 (1994).

[5] E. K. Hulet, *Phys. At. Nucl.* **57**, 1099 (1994).

[6] S. Antalic, et al., *Eur. Phys. J. A* **51**, 41 (2015).

[7] B. Sulignano, et al., *Eur. Phys. J. A* **33**, 327 (2007).

[8] A. Ghiorso, et al., *Phys. Rev. C* **7**, 2032 (1973).

[9] R. D. Herzberg, et al., *Nature* **442**, 896 (2006).

[10] F. P. Heßberger, et al., *Eur. Phys. J. A* **43**, 55 (2009).

[11] H. M. David, et al., *Phys. Rev. Lett.* **115**, 132502 (2015).

[12] H. B. Jeppesen, et al., *Phys. Rev. C* **79**, 031303 (2009).

[13] A. P. Robinson, et al., *Phys. Rev. C* **83**, 064311 (2011).

[14] A. Lopez-Martens, et al., *Eur. Phys. J. A* **32**, 245 (2007).

[15] S. Antalic, et al., *Eur. Phys. J. A* **47**, 62 (2011).

[16] S. Antalic, et al., *Eur. Phys. J. A* **38**, 219 (2008).

[17] K. Hauschild, et al., *Phys. Rev. C* **78**, 021302 (2008).

[18] J. Rissanen, et al., *Phys. Rev. C* **88**, 044313 (2013).

[19] V. E. Viola, *Nuclear Data Sheets. Section A* **1**, 391 (1965).

[20] Yu. Ts. Oganessian, *J. Phys. G* **34**, R165 (2007).

[21] P. Walker, G. Dracoulis, *Nature* **399**, 35 (1999).

[22] K.E.G. Löbner, *Phys. Lett. B* **26**, 369 (1968).

[23] S. Hofmann, et al., *Eur. Phys. J. A* **10**, 5 (2001).

[24] GSI, *Helmholtz Centre for Heavy Ion Research*, https://www.gsi.de.

[25] S. Hofmann, G. Münzenberg, *Rev. Mod. Phys.* **72**, 733 (2000).

[26] S. Hofmann, et al., *Eur. Phys. J. A* **52**, 116 (2016).

[27] Š. Šáro, et al., *Nucl. Instrum. Meth. A* **381**, 520 (1996).

[28] S. Hofmann, et al., *Eur. Phys. J. A* **32**, 251 (2007).

[29] S. Hofmann, et al., *Z. Phys. A* **291**, 53 (1979).

[30] G. Münzenberg, et al., *Nucl. Instrum. Meth.* **161**, 65 (1979).

[31] F. P. Heßberger, et al., *Eur. Phys. J. A* **52**, 328 (2016).

[32] F. P. Heßberger, et al., *Z. Phys. A* **322**, 557 (1985).

[33] K. Nishio, et al., *AIP Conf. Proc.* **891**, 71 (2007).

[34] B.D. Wilkins, et al., *Nucl. Instrum. Meth.* **92**, 381 (1971).

[35] O. B. Tarasov, D. Bazin, *Nucl. Instrum. Meth. B* **266**, 4657 (2008).

[36] F. P. Heßberger, et al., *Eur. Phys. J. A* **30**, 561 (2006).

[37] M. Vostinar, et al., *Eur. Phys. J. A* **55**, 17 (2019).

[38] R. R. Chasman, et al., *Rev. Mod. Phys.* **49**, 833 (1977).

[39] P. Möller, et al., *Atom. Data Nucl. Data Tabl.* **109-110**, 1 (2016).

[40] P. Mosat, et al., *Acta Phys. Pol. B* **49**, 605 (2018).

[41] P. Mosat, et al. submitted to Phys. Rev. C, 2019.